Membrane lipid poly-unsaturation selectively affects ligand induced dopamine D2 receptor internalization

Rim Baccouch, Silvia Sposini, Véronique De Smedt-Peyrusse, Joyce Heuninck, Thierry Durroux, Pierre Trifilieff, David Perrais, Isabel Alves

Membrane lipid poly-unsaturation selectively affects ligand induced dopamine D2 receptor internalization

Rim Baccouch[1]*, Silvia Sposini[2,3]*, Véronique De Smedt-Peyrusse[4], Joyce Heuninck[5], Thierry Durroux[5], Pierre Trifilieff [4#], David Perrais[2#], Isabel Alves[1#]

[1] CBMN, CNRS UMR 5248, Allée Geoffroy St Hilaire, 33600 Pessac, France

[2] IINS, CNRS UMR 5297, 146 rue Léo-Saignat, 33076 Bordeaux, France

[3] IRDB, Department of Metabolism, Digestion and Reproduction, Imperial College London, London, United Kingdom

[4] Université de Bordeaux, INRAE, Bordeaux INP, NutriNeuro, 33000, Bordeaux, France.

[5] IGF, Université de Montpellier, CNRS, Inserm

*equal contribution

[#]corresponding authors: pierre.trifilieff@inrae.fr; david.perrais@u-bordeaux.fr; i.alves@cbmn.u-bordeaux.fr

Keywords

Endocytosis; poly-unsaturated fatty acid; β-arrestin; β-adrenergic receptor; TIRF microscopy

Abstract

The poly-unsaturation of membrane phospholipids is an important feature for the biophysical properties of membranes and membrane proteins. In particular, it regulates the function of some G protein-coupled receptors (GPCR), such as their binding to ligand and G proteins or their membrane diffusion. However, its effects on GPCR internalization and trafficking remain unknown. The brain is highly enriched in poly-unsaturated fatty acids (PUFAs) and ω3-PUFAs deficiency has been associated with several neuropsychiatric disorders. Importantly, the Dopamine D2 receptor (D2R), a class A GPCR, is consistently impacted in these disorders and represents the main target of most antipsychotics. Here we show that enrichment in two different PUFAs strongly impairs agonist-induced endocytosis of D2R in HEK293 cells, without affecting clathrin-mediated endocytosis or β2 adrenergic receptor endocytosis. Using live cell TIRF imaging, we show that D2R clustering is not affected, but that recruitment of β-arrestin2 is strongly impaired and endocytic vesicle formation is slowed down. We conclude that PUFAs are involved in D2R trafficking, which could influence its role in the control of brain activity and behavior.

Introduction

Cell signaling events almost systematically involve a complex interplay between protein and membrane remodeling. In particular, lipids are key regulators of membrane protein structure, conformational flexibility and activity. For example, the activity of many G protein coupled receptors (GPCRs), the largest family of membrane receptors, such as rhodopsin, the serotonin $5HT_{1A}$ receptor or the chemokine CCR5 receptor, is strongly influenced by the presence of cholesterol in the membrane (Calmet *et al*, 2020; Pucadyil & Chattopadhyay, 2004; Jastrzebska *et al*, 2011; Pontier *et al*, 2008). Moreover, the nature of phospholipid headgroups (phosphatidylcholine or phosphatidylethanolamine) also affects the binding of agonists or antagonists to GPCRs and their activation such as for the β2 adrenergic receptor (β2AR) (Dawaliby *et al*, 2016). Finally, the nature of the fatty acid chains of phospholipids may also affect GPCR activity. For rhodopsin and adenosine A_{2A} receptors, the poly-unsaturated fatty acid (PUFA) docosahexaenoic acid (ω3-DHA) is necessary for preserving their optimal conformation and activity (Mitchell *et al*, 1992; Niu *et al*, 2004; Grossfield *et al*, 2006; Mizumura *et al*, 2020).

PUFAs are fatty acid species that contain two or more unsaturations in their carbon chain. In the brain, PUFAs accumulate during *in utero* development and constitute roughly 30 % of total brain lipids in adulthood where they can modulate membrane properties, signaling pathways, and cell metabolism (Bazinet & Layé, 2014). Deficits in brain PUFA accumulation have been linked to several psychiatric disorders including major depressive disorder, bipolar disorder or schizophrenia (Garland *et al*, 2007; Berger *et al*, 2006). In particular, lower levels of ω3-PUFAs in the brain of individuals suffering from psychiatric disorders have been described (McNamara *et al*, 2007b, 2007a, 2008) and some studies have reported a significant advantage of ω3-PUFAs dietary supplementation for reducing symptoms (Robinson *et al*, 2019; Grosso *et al*, 2014). However, the molecular mechanisms by which PUFAs participate in the etiology of psychiatric symptoms remain largely elusive.

A common neurobiological phenotype found across many psychiatric disorders is a dysfunction in dopamine transmission, in particular, the activity of the dopamine D2 receptor (D2R) (Whitton *et al*, 2015; Beaulieu & Gainetdinov, 2011). Interestingly, ω3-PUFA deficiency in animal models have revealed alterations of dopamine transmission (Chalon, 2006) and a particular vulnerability of D2R-expressing neurons to ω3-PUFAs deficiency (Ducrocq *et al*, 2020). Mechanistically, molecular dynamics simulations show that membrane PUFA levels modulate the membrane diffusion rate of the D2R (Guixà-González *et al*, 2016).

Moreover, enrichment in PUFAs in HEK 293 cells alters D2R ligand binding and signaling (Jobin *et al*, 2023). Altogether, these findings suggest a direct link between membrane PUFAs and the activity of the D2R.

Like many GPCRs, the signaling efficiency mediated by D2R is directly related to the overall number of responsive receptors at the cellular membrane, which is controlled by internalization and desensitization processes. Specifically, activation by agonists leads to D2R phosphorylation by G protein receptor kinase 2/3 (GRK 2/3) on serine and threonine residues in the second and third intracellular loops. This phosphorylation triggers robust recruitment of a cytoplasmic protein, β-arrestin2, which binds and targets the phosphorylated receptor by scaffolding it to clathrin-coated pits (CCPs), leading to its internalization into endosomes after dynamin-dependent membrane scission (Kim *et al*, 2001; Lan *et al*, 2009; Skinbjerg *et al*, 2009; Paspalas *et al*, 2006). Furthermore, β-arrestins also function as scaffold proteins that interact with cytoplasmic proteins and link GPCRs to intracellular signaling pathways such as MAPK cascades (Gurevich & Gurevich, 2006; Jean-Alphonse & Sposini, 2021). Therefore, membrane lipid composition, in PUFAs in particular, which affect membrane biophysical properties (Barelli & Antonny, 2016; Baccouch *et al*, 2023), is likely to affect GPCR trafficking.

Here we investigated the modulatory effect of membrane lipid poly-unsaturation on ligand-induced D2R internalization. D2R-expressing HEK 293 cells were treated with either the ω3-PUFA DHA or the ω6-PUFA docosapentaenoic acid (DPA) in order to increase membrane poly-unsaturation in a controlled manner. Using resonance energy transfer-based technique or confocal microscopy, we demonstrated that PUFA membrane enrichment strongly blunted ligand-induced internalization of D2R but did not affect the internalization of two other transmembrane receptors, the β2AR (a class A GPCR as the D2R) and the transferrin receptor (TfR). In addition, we found using Total Internal Reflection fluorescence (TIRF) microscopy that ligand-induced clustering of D2R was preserved in PUFA-enriched cells but that β-arrestin2 membrane recruitment was impaired under PUFA enrichment.

Results

Robust incorporation of exogenous FAs into cell membranes

To assess the potential effects of membrane PUFAs on D2R trafficking, we used the protocol developed in (Jobin *et al*, 2023) to enrich membrane phospholipids with selected FAs, namely

DHA, DPA and the saturated fatty acid (SFA) behenic acid (BA), that displays the same carbon chain length (22) as DHA and DPA (Figure EV1A). Incubation with 30 µM of DHA or DPA increased the contents of PUFAs in phospholipids, from 8.6 % in control (EtOH) to ~14 % in cells treated with DHA or DPA (Figure EV1B), while incubation with 30 µM of BA increased the content of SFA in phospholipids from 34.7% in control (EtOH) to 39.7% in BA treated cells (Figure EV1C). DHA and DPA were specifically enriched after their respective treatments (Figure EV1D), while BA treatment, enriched phospholipids in SFAs (Figure EV1E). Consequently, the ratio of total ω6 (such as DPA) and ω3 (such as DHA) PUFAs (ω6/ω3) was significantly changed for cells treated with DHA (3-fold lower, $p < 0.01$) or DPA (2.7-fold higher, $p < 0.0001$), but not for cells treated with BA (Figure EV1F). Despite the significant incorporation of these exogenous FAs into membrane lipids, these treatments did not induce any cell toxicity (Figure EV1G), nor affected the level of expression of transfected tagged D2R (Figure EV1H).

Impact of PUFA enrichment on D2R internalization investigated by DERET assay

We assessed the effect of PUFA enrichment on the internalization of D2R induced by multiple ligands in a dose-response manner using a high-throughput fluorometric assay, diffusion-enhanced resonance energy transfer (DERET) (Levoye *et al*, 2015). Agonist-induced SNAP-D2R internalization resulted in an increase in the fluorescence ratio R (620/520 nm), which corresponds to a loss of energy transfer between internalized receptors and extracellular fluorescein (Figure EV2A). Application of the endogenous D2R agonist dopamine (10 µM) resulted in a strong increase in R over time that was reversed by addition of the D2R antagonist haloperidol or partial agonist aripiprazole (at 10 and 100 µM concentration, respectively) 45 minutes after dopamine application (Figure EV2B,C). These latter findings are likely to result from the blocking effects of haloperidol and aripiprazole on dopamine-induced D2R internalization, and to the recycling of the internalized D2R population to the cell surface. Taken together, these results confirm that DERET assay is a suitable technique to monitor agonist-induced D2R internalization in real time.

We next investigated the impact of membrane PUFA (DHA, DPA) or SFA (BA) enrichment on agonist-induced D2R internalization. Importantly, these treatments did not affect the level of D2R surface expression, as measured by SNAP-Lumi4-Tb fluorescence intensity at 620 nm (donor fluorescence) (Figure EV1H). However, enrichment with either PUFAs (DHA or DPA) strongly blunted D2R internalization induced by either dopamine or quinpirole (Figures

1A,B). This effect of PUFAs was observed for all tested agonist concentrations, 30 min after dopamine or quinpirole stimulation. Dose-response curves revealed a significant reduction of the maximal response (E_{max}) for PUFA-enriched cells (Figures 1C-E). However, no significant difference in dopamine-induced internalization efficacy (EC_{50}) was observed under membrane PUFA enrichments, while EC_{50} for quinpirole was significantly higher when compared to control cells (Figure 1F). These same results were confirmed with dose-response curves obtained at later times following agonist application (Figure EV3). Conversely, treatment with BA did not affect D2R internalization induced by neither dopamine nor quinpirole (10 µM) (Figure 1G, H). Altogether, these data indicate that the decrease in D2R internalization after membrane PUFA enrichment is not related to the increased amount of long chain FAs (C22) but rather to the increased levels of membrane poly-unsaturation, independently of the nature of the PUFA chain (i.e. ω3 vs. ω6).

PUFA levels selectively affect D2R internalization without affecting general endocytosis

To get insight on the cellular mechanisms underlying blunted D2R ligand-induced internalization under membrane PUFA enrichment, we analyzed the steps of receptor internalization following agonist binding: D2R clustering at endocytic pits, recruitment of β-arrestin2 and formation of endosomes (Tsao & von Zastrow, 2000; Sposini & Hanyaloglu, 2018). We first examined the formation of endosomes with confocal microscopy. Cells expressing FLAG-D2R, GRK-2 and β-arrestin2 were labelled live with anti-FLAG antibody for 10 min, incubated with or without D2R agonists (dopamine or quinpirole) for 30 min, quickly washed in PBS/EDTA solution to remove surface bound antibodies, and fixed. As shown in Figures 2A and C, in the absence of D2R agonists, FLAG staining was mostly restricted to the cell periphery, suggesting that the D2R has little constitutive internalization in all conditions of PUFA treatment. Addition of D2R agonists greatly increased the formation of punctuate structures corresponding to internalized receptors in untreated cells (3.75 and 18-fold increase in puncta number, respectively, upon dopamine and quinpirole stimulation, $p < 0.0001$). However, in DHA and DPA treated cells, the number of puncta induced by dopamine was much smaller (34.5 ± 6.12 % and 29.5 ± 6 % of control for DHA and DPA, respectively, $p < 0.0001$) (Figure 2A, B). Similar results were obtained in cells treated for 30 min with the selective D2 agonist quinpirole (61.8 ± 6.9 % of control for DHA and 48.5 ± 7.3 % DPA, respectively, $p < 0.0001$) (Figure 2C, D). These results further show that cell enrichment with either PUFAs dampens agonist-induced D2R internalization.

To examine whether the effect of DHA or DPA treatment was specific for the D2R or rather a more general mechanism for class A GPCRs, we examined the internalization of β2 adrenergic receptors (β2ARs) following agonist stimulation (Goodman *et al*, 1996). As shown in Figure 3A, the FLAG-tagged β2AR was mostly localized at the cell surface in the absence of agonist and internalized after addition of the selective agonist isoproterenol (10 µM). In striking difference with the results obtained with the D2R, the number of puncta was similar in control and PUFA-enriched cells (107 % and 101 % of control for DHA and DPA, respectively, $p > 0.05$) (Figure 3B). Altogether, these results suggest that the effect of PUFA enrichment on internalization is not a general mechanism for class A GPCRs.

Like many GPCRs, D2R and β2AR are internalized through clathrin-mediated endocytosis (CME) (Paspalas *et al*, 2006; Goodman *et al*, 1996; von Zastrow & Kobilka, 1994). We then tested if PUFA treatment affected the internalization of transferrin, a prototypical CME cargo (Doherty & McMahon, 2009). Fluorescently-labeled transferrin (Tfn-A568) uptake was assessed by confocal microscopy in both control and PUFA-enriched cells, incubated for 5 min at 37 °C in presence of Tfn-A568. As shown if Figure 3C, D, treatment with either PUFA did not affect the number of Tfn-Alexa568 puncta after internalization for 5 min (105 % and 106 % of control for DHA and DPA, respectively, $p > 0.05$). Taken together, these results support that the specific effect of both PUFAs on ligand-induced D2R internalization is not due to an alteration of CME.

Membrane PUFAs do not alter D2R clustering but reduce the recruitment of β-arrestin2 and D2R endocytosis

Upon agonist stimulation, β-arrestin2 (βarr2) is recruited from the cytoplasm to activated D2R (Beaulieu *et al*, 2005; Skinbjerg *et al*, 2009). Once recruited, βarr2 clusters at CCPs (Goodman *et al*, 1996), while class A GPCRs cluster at CCPs with varying degrees (Eichel *et al*, 2018). Therefore, we investigated D2R clustering and β-arr2 recruitment in cells transfected with D2R tagged with superecliptic pHluorin (SEP), a GFP mutant which is not fluorescent at pH 5.5, GRK-2 and βarr2-mCherry and imaged live with TIRF microscopy. As shown in Figure 4A and Movies EV1-3, SEP-D2R signal in control and PUFA-enriched cells was initially homogenous on the plasma membrane, then clustered following quinpirole stimulation. We quantitatively assessed this accumulation by measuring the fluorescence intensity at SEP-D2R clusters. Fluorescence quickly increased immediately after agonist application to reach a peak within ~100 s and slowly decreased thereafter (Figure 4B). The peak of SEP-D2R recruitment was not significantly different in control and PUFA-enriched

cells (Figure 4C). βarr2-mCherry was also recruited to SEP-D2R clusters following agonist application (Figure 4D-F). However, PUFA treatment significantly decreased βarr2-mCherry recruitment without affecting its recruitment kinetics (Figure 4D, G). Similar results were obtained with cells treated with dopamine (Figure EV4).

We next tested SEP-D2R endocytosis directly with the pulsed pH (ppH) protocol (Sposini *et al*, 2020). In the ppH protocol, cells are perfused alternatively every 2 s with buffers at pH 7.4 and 5.5. At pH 5.5, SEP-D2Rs on the plasma membrane are not fluorescent, revealing forming endocytic vesicles (Figure 5A). Endocytic vesicles containing SEP-D2R were thus detected by the ppH protocol in images at pH 5.5 at preexisting SEP-D2R clusters, visible at pH 7.4, as shown in an example event (Figure 5B). Following quinpirole application, SEP-D2R and βarr2-mCherry clusters formed (Figure 5C), like in cells without pH changes (see Figure 4). Moreover, endocytic events were detected essentially following agonist application (Figure 5C middle, Figure 5D and Movie EV4). While PUFA treatments did not change the number of clusters detected after quinpirole application (Figure 5E), it significantly decreased the frequency of endocytic events detected by the ppH protocol (Figure 5F). We then determined the fluorescence of SEP-D2R at the time of vesicle detection. It was affected neither at pH 7.4, reflecting the number of receptors in clusters (Figure 5G), nor at pH 5.5, reflecting the number of receptors in endocytic vesicles (Figure 5H). Moreover, averages of fluorescent traces aligned on vesicle detection (time 0) revealed that the kinetics of endocytic events were not affected by PUFA treatments (Figure 5J, K). Finally, the fluorescence of βarr2-mCherry at SEP-D2R clusters was significantly decreased in both DHA and DPA treated cells, but the kinetics of recruitment before or after vesicle detection was not different (Figure 5I, L).

Discussion

The fatty acid composition of membrane lipids could affect its biophysical properties. Indeed, we have recently shown that enrichment of HEK 293 cells in DPA, but not DHA, affects the elasticity and fluidity of the plasma membrane (Baccouch *et al*, 2023). Similarly, incorporation of DHA in RPE-1 cells affects their membrane bending rigidity (Pinot *et al*, 2014). Molecular dynamics simulations and biochemical measurements suggest that DHA-containing phospholipids adapt their conformation to membrane curvature via their higher flexibility and make the plasma membrane more amenable to deformation by decreasing its bending rigidity (Manni *et al*, 2018). Consequently, Tfn endocytosis was increased in RPE-1 cells (Pinot *et al*, 2014). Despite a similar level of PUFA enrichment in our protocol (Jobin et al. 2023; Baccouch et al. 2023; this study) and in Pinot et al. (2014), we found that PUFA enrichment in HEK 293 cells did not affect Tfn internalization, arguing against a general effect of PUFA enrichment on endocytosis. Instead, PUFA enrichment specifically inhibits D2R endocytosis, leaving the endocytosis of another class A GPCR, β2AR, unaffected.

We can envision three possible mechanisms for the selective inhibition of D2R internalization by PUFAs. Firstly, PUFA-containing phospholipids could specifically interact with and form a corona around D2Rs within the plasma membrane, affecting its conformation or diffusion in the plasma membrane. This possibility is corroborated by molecular modelling showing that PUFA tails preferentially interact with the D2R when compared to saturated ones (Guixà-González *et al*, 2016; Jobin *et al*, 2023). Such a preferential interaction with polyunsaturated chains of phospholipids has been described, using molecular modelling approaches, for other class A GPCRs including rhodopsin (Soubias *et al*, 2006) and the adenosine A_{2A} receptor (Leonard & Lyman, 2021; Yang & Lyman, 2019). Further work is needed to determine whether the effect of membrane PUFA on internalization is specific to the D2R or if other GPCRs share common properties, and, if so, whether this results from comparable molecular interactions between PUFAs and the receptor.

Secondly, PUFA enrichment could affect the interaction between D2R and associated proteins. Indeed, we show that PUFA enrichment decreases agonist-induced β-arrestin2 recruitment to receptor clusters at the membrane, a main step for internalization of many GPCRs including the D2R (Skinbjerg *et al*, 2009; Clayton *et al*, 2014; Del'guidice *et al*, 2011). Even though very little data exist regarding PUFAs, increasing evidence show that

membrane lipids, especially anionic ones, like phosphatidylinositol phosphates (PIPs), participate to GPCR/effector interaction. PIPs have been shown to be crucial for the recruitment of β-arrestins to some GPCRs (Sommer *et al*, 2006; Janetzko *et al*, 2022), namely via the TM3 (Pluhackova *et al*, 2021), by facilitating the activation of β-arrestin as well as its interaction with receptors (Janetzko *et al*, 2022). Moreover, anionic lipids were also shown to modulate the recruitment of GRKs to GPCRs, and therefore receptor phosphorylation, which is crucial for β-arrestin recruitment (Komolov *et al*, 2017). Such key positioning of anionic lipids in GPCR/effector interfaces has been revealed by high resolution structures of such complexes (Thakur *et al*, 2023; Xu *et al*, 2021). Most of those structures have been obtained by cryo-electron microscopy, a technique that still fails to resolve lipid fatty acid chain regions. It is thus possible that membrane enrichment in PUFAs could influence arrestin/receptor interaction as well as GRK activity either directly through allosteric modulation, or indirectly by altering acidic and/or charged phospholipids. While the potential impact of PUFA enrichment in the D2R/β-arrestin interface region remains to be determined, molecular modelling studies of our recent work have revealed a substantial impact of PUFAs on the conformational flexibility of the D2R, both around extracellular loops implicated in ligand binding and in β-arrestin recognition (Jobin *et al*, 2023). Specifically, part of the second intracellular loop (ICL2), comprising two serine residues that can be potentially phosphorylated, is hidden in PUFA-rich membrane and becomes exposed in PUFA-poor membrane, providing hints for the molecular mechanisms behind the PUFA effect in D2R internalisation.

Thirdly, the level of PUFAs in membrane phospholipids could impact membrane compartmentalisation in lipid nanodomains, which may result in decreased encounters between the receptor and β-arrestin2 and/or GRK, a necessary step for GPCR trafficking (Grimes *et al*, 2023). Indeed, plasma membrane microdomains, especially lipid rafts, are known to regulate cell signalling by clustering both the receptor and its signalling machinery such as heterotrimeric G proteins (Oh & Schnitzer, 2001; Villar *et al*, 2016; Fallahi-Sichani & Linderman, 2009). Moreover, disruption of lipid raft formation abolishes signalling from certain GPCRs, including a class A GPCR, the NK1 receptor (Monastyrskaya *et al*, 2005). Thus, β-arrestin2 reduced recruitment could result from PUFA-induced alteration in lipid membrane compartmentalisation, hindering potential β-arrestin2/D2R encounters.

Finally, in substantia nigra pars compacta dopaminergic neurons, which strongly express D2Rs, internalization of the receptors in brain slices following agonist application (dopamine

or quinpirole) was very limited, whereas another GPCR, μ-opioid receptor, substantially internalized following agonist application in the same neurons (Robinson *et al*, 2017). Interestingly, in the same study, D2Rs ectopically expressed in locus coeruleus neurons strongly internalized following agonist application (Robinson *et al*, 2017). Although a number of associated signalling and scaffold proteins could regulate D2R trafficking following agonist binding, the present study raises the possibility that such an effect could be in part due to different PUFA composition between neuronal subtypes. In conclusion, our results point to a potential mechanism by which lower PUFA levels described in several psychiatric disorders could directly participate in the aetiology of the diseases. Moreover, because PUFA levels can be modified, notably by dietary intake, the observation that PUFAs can directly alter the functionality and activity of the D2R pave the way for novel strategies to ameliorate the efficacy of classical pharmacological treatments such as antipsychotics for which the D2R is a main target.

Materials and methods

Cell culture and transfection

HEK-293 cells (ECACC, #12022001) were grown in DMEM supplemented with 10% Fetal Calf Serum and 1% penicillin/streptomycin in a 5% CO_2 enriched atmosphere at 37°C. Cells were passed twice a week and used between passages 8 and 20. HEK-293 cells were transfected with Lipofectamine®2000 for transient expression of tagged D2R short (or β2AR), β-arrestin2 and GRK-2 with parameters adapted for the experiment (see below). SNAP-D2R was purchased from Cisbio bioassays and FLAG-β2AR was described previously (Sposini *et al*, 2017). SEP-D2R was obtained based on SEP-LHR and FLAG-D2R constructs described previously in (Sposini *et al*, 2017) and (Guo *et al*, 2008), respectively. SEP was subcloned from SEP-LHR using AgeI and ligated into FLAG-D2R, containing an AgeI restriction site in the FLAG sequence created by site-directed mutagenesis (QuikChange Mutagenesis kit, Agilent) using oligonucleotides detailed in Reagents and Tools table.

For diffusion-enhanced resonance energy transfer (DERET) assays, cells were transfected as follows. White polyornithine 96-well plates were coated with poly-L-lysine (PLL, 50 µl of 0.1 mg/ml) for 30 min at 37°C, then washed twice with 100 µL sterile phosphate buffered saline solution (PBS). After the washing step, a transfection mixture (50 µl/well) composed of 0.5 µl of Lipofectamine®2000, 5 ng of each of the following plasmids (N-terminal SNAP tagged D2R, GRK-2 and β-arrestin2) and 185 ng of an empty vector were prepared in Opti-MEM reduced serum medium. After 20 min incubation at room temperature (RT), the DNA/lipofectamine mixture was added to each well and followed by 100 µl of HEK-293 cells at a density of 250,000 cells/ml. Cells were grown 24 hours at 37°C before the addition of PUFAs for 24 h before the DERET measures.

For confocal and TIRF microscopy experiments, cells were seeded in a 6 well plate in order to reach approximately 70 % confluence on the day of the transfection. Cells were transfected with a mixture (0.5 ml/well) containing 5 µl of Lipofectamine®2000 and 150 ng of each of the following DNA (the N-terminally FLAG-tagged D2R or FLAG-β2AR, the GRK-2 and the β-arrestin2) diluted in Opti-MEM medium and added dropwise to each well. For TIRF microscopy, cells were transfected with 150 ng of SEP-D2R, mCherry-β-arrestin2 (Boularan *et al*, 2007) and GRK-2. Transfected cells were grown for 24 h at 37°C before incubation with PUFAs for another 24 h.

Cell fatty acid treatment and analysis

Fatty acids (FAs) were dissolved in absolute ethanol under nitrogen at 30 mM and stored in aliquots until use. Cells were incubated with the different FAs as in (Jobin *et al*, 2023). Specifically, aliquots of each FA were diluted in complete DMEM for a final concentration of 30 µM with a final fraction of 0.1% ethanol (EtOH, vehicle for control cells) for 24 h. Following incubation, cells were rinsed with complete DMEM to remove excess of FAs.

In order to ascertain exogenous FAs (BA, DHA, DPA) incorporation, whole cell FAs analysis was performed as in (Jobin *et al*, 2023). Briefly, control and FAs treated cells were randomly analyzed according to (Joffre *et al*, 2016). Total lipids were extracted according to the method developed by (Folch *et al*, 1957) and transmethylated using 7 % boron trifluoride in methanol following (Morrison & Smith, 1964) protocol. Fatty acid methyl esters (FAMEs) were extracted and analyzed by gas chromatography-flame ionization detector (GC-FID, Hewlett Packard HP5890, Palo Alto, CA). FAMEs were identified by comparison with commercial and synthetic standards and data analysis were processed using the Galaxie software (Varian). The proportion of each FA was expressed as a percentage of total fatty acids to allow the comparison of lipid composition in different cell culture conditions.

Cell viability assay

Cell viability was measured using Resazurin Fluorimetric Cell Viability Assay. One day after ethanol, DHA, DPA or BA treatments, control (ethanol) and FAs enriched cells were washed gently twice with pre-warmed PBS, and then a mixture of resazurin and DMEM in a ratio 1:10 was added into each well. After 3 h incubation at 37 °C, cell viability was monitored by measuring fluorescence with λ_{ex} at 540 nm and λ_{em} at 590 nm in a Tecan infinite M1000 Pro reader. The fluorescent signal generated in each well is directly proportional to the number of living cells in the sample. The percentage of survival of FA-treated cells was calculated relative to control (EtOH)-treated cells.

DERET assay and data analysis

Internalization assay was performed in white 96-well culture cell plates, using D2R, GRK-2, β-arrestin2 transfected and FAs enriched HEK-293 cells, as described above. Cell culture medium was removed 24 h after PUFA treatment and 100 nM of SNAP-Lumi4-Tb (the donor fluorophore) previously diluted in Tag-lite buffer was added (50 µl/well) and further

incubated for 1h at 16 °C to prevent/minimize receptor internalization. Excess SNAP-Lumi4-Tb was removed by washing each well four times with 100 µl of Tag-lite labeling buffer.

Membrane expression levels of the receptor were determined by measuring the fluorescence intensity of D2R-SNAP-Lumi4-Tb at 620 nm. Internalization experiments were performed by incubating cells with Tag-lite labeling buffer, either alone or containing one of the D2R ligands (Dopamine, Quinpirole, Aripiprazole, Haloperidol) in the presence of fluorescein (fluorescence acceptor). Typically, in plates containing SNAP-Lumi4-Tb-labeled cells, 90 µl of 25 µM fluorescein was added followed by the addition of 10 µl of ligand to reach a final concentration in the well ranging from 10^{-14} to 10^{-4} M. Fluorescence measurements were performed in a Tecan Infinite M1000 Pro plate reader, at 37°C right after the treatment described above.

For the experiments assessing D2R internalization kinetics, cells were stimulated with 10 µM of ligand. For dose response experiments, signals emitted by the donor (Lumi4-Tb) at 620 nm and by the acceptor (fluorescein) at 520 nm were collected at the indicated time points using time-resolved settings for the donor (1500 µs delay, 1500 µs reading time) and acceptor (150 µs delay, 400 µs reading time). The fluorescence intensity ratio 620/520 (R) was obtained by dividing the donor fluorescence signal (measured at 620 nm) by the acceptor fluorescence signal (measured at 520 nm) at a chosen time.

Data are expressed as percent of maximal internalization [% of max. internalization (620/520 nm)] using the following equation: $[(R_t - R_{min})/ (R_{max} - R_{min})] \times 100$ where R_t corresponds to the ratio observed at a chosen time, R_{min} and R_{max} correspond, respectively, to the minimum and the maximum fluorescence ratios. Data expressed in dose-response curves were fitted using non-linear regression dose-response and the following equation: Y=Bottom + X*(Top-Bottom) / (EC_{50} + X), where X and Y represent the ligand concentration (log scale) and the maximum internalization (in percentage) allowing to obtain both the maximal effect (Emax) and half maximal effective concentration (EC_{50}) values.

Confocal microscopy imaging and data analysis

24 h before confocal imaging, glass slides were placed in a 12-well plate and coated with PLL (250 µl of 0.1 mg/ml) for 30 min at 37 °C. After coating, HEK-293 cells transiently expressing the FLAG-D2R, GRK-2 and β-arrestin2 (or FLAG-β2AR, GRK-2 and β-arrestin2) were seeded in complete DMEM containing 30 µM of PUFA or 0.1 % of EtOH. Cells were kept at 37 °C, 5% CO_2 for 24 hours to allow PUFA incorporation into cells.

For fixed cell imaging, cells were incubated with M1 anti FLAG antibody (1:500) for 10 min at 37° C and then left untreated or stimulated with 10 µM D2R or β2AR ligands (dopamine or quinpirole for D2R, isoproterenol for β2AR) for 30 min. Unstimulated cells were then washed with PBS (pH 7.4 containing 0.9 mM of Ca^{2+}), whilst stimulated cells were washed three times with PBS/0.04% EDTA to remove FLAG antibody bound to the remaining surface receptors. Cells were then immediately fixed with 4% (v/v) paraformaldehyde diluted in Ca^{2+} enriched PBS for 10 min at RT. Fixed cells were permeabilized with 0.2% (v/v) Triton-X for 10 min and incubated with Alexa Fluor-555 anti-mouse antibody (1:1000) for 30 min at RT in the dark. Cells were washed 3 times with PBS and the coverslips were mounted on glass slides using Fluoromount.

Images were acquired with a spinning-disk confocal microscope (Leica DMI 6000B) controlled with MetaMorph (Molecular Devices), equipped with an EMCCD evolve camera and 561 nm diode laser. Images were analyzed using MetaMorph software and MatLab2018a (MathWorks). Z-stack of twelve images separated with a fixed step size of 0.5 µm were acquired with a 63×/1.4 NA oil immersion objective. The maximal projections of the z-stacks were used to quantify the internalized receptors. A mask was traced around each cell as well as a background region using MetaMorph. Generated clusters of internalized receptors (FLAG-D2R or FLAG-β2AR) were detected by wavelet segmentation using custom written Matlab programs. For each cell, the number of clusters per mask was computed using a homemade Matlab script. These numbers were normalized to 100 for the control condition (cells grown in absence of PUFAs and treated with receptor's agonists) for each of the 3 independent experiments performed.

For live cell imaging, receptor trafficking was monitored by incubating the cells in FluoroBrite DMEM containing the M1-FLAG antibody (10 min, 37 °C, 5 % CO2) followed by Alexa Fluor-555 anti-mouse antibody (10 min, 37 °C, 5 % CO_2). Then cells were washed 3 times with the same medium, maintained at 37 °C and 5 % CO_2 using an environmentally controlled incubation chamber and imaged for 45 min. Images were acquired using the same microscope described above and live images were taken every 60 s for 45 min at the equatorial cell plane. After 5 min recording, receptor internalization was induced by agonist addition (10 µM) directly into the imaging medium.

Transferrin uptake assay

HEK-293 cells endogenously expressing TfR were seeded on PLL coated glass coverslips and incubated with PUFAs as described above. After 24 h, cells were serum starved in pre-warmed DMEM for 30 min and then incubated for 15 min in cold DMEM containing 10 µg/ml Alexa Fluor 568-conjugated transferrin (Tfn-A568). Cells were incubated 5 min at 37 °C, allowing Tfn-A568 internalization, and washed in cold DMEM then in cold glycine buffer (100 mM NaCl, 50 mM glycine, pH 3) for 2 min to remove Tfn-A568 bound to non-internalized TfR (stripping). Stripped cells were then fixed as explained above and kept at 4 °C until imaging. Fixed cell imaging and cluster quantification were performed in the same manner as described above for the GPCRs.

TIRF microscopy imaging and data analysis

Cells transiently expressing SEP tagged D2R, GRK-2 and β-arrestin2-mcherry were plated on PLL coated glass coverslips, grown in complete DMEM and then enriched with PUFAs as described above. 48 h after transfection and 24 h after PUFA enrichment, live cells were washed 2 times with FluoroBrite™ and imaged for 10 min in the same medium. The indicated D2R agonist was added at time 120 s, for experiments shown in time-courses. Live TIRF imaging was performed at 37°C in a temperature-controlled chamber under constant flow on a motorized Olympus IX83 inverted microscope outfitted with TIRF illuminator (Ilas2, Gataca Systems) with fiber coupled Laser sources (Cobolt Lasers 06-DPL 473 nm, 100 mW and 06-MLD 561 nm, 50 mW). Images were obtained with an Olympus TIRF objective (150X, 1.45 NA, oil immersion). Dual channel live acquisition was performed using 2 EMCCD cameras (QuantEM Model 512SC, Princeton Instruments) controlled by Metamorph 7.10 software (Molecular Devices). The gain of the EMCCD cameras was kept constant at 600, binning at 1 × 1, readout speed 10 MHz. Time lapse image sequences were acquired for up to 20 minutes at 0.5 Hz with an exposure time of 100 ms. Images of fluorescent beads (Tetraspeck microspheres, 0.2 µm) were acquired in every experiment as described previously (Sposini *et al*, 2020). Microbeads images were used to determine the precise parameters required for alignment of the two cameras; these parameters were then applied to all the images acquired on that day.

To quantify changes in β-arrestin2-associated mCherry fluorescence as a proxy of plasma membrane recruitment and D2R-associated SEP fluorescence as a proxy for D2R clustering, fluorescence values measured during the 60 frames before dopamine or quinpirole addition were averaged and subtracted from fluorescence values measured at each frame (1-300)

within an ROI drawn around each generated cluster. Quantitative image analysis was performed using MatLab2018a software.

Pulsed pH (ppH) protocol

Cells transfected and enriched in PUFAs as described in the paragraph above were perfused with HEPES buffered saline solution (HBS) at 37 °C. HBS contained, in mM: 135 NaCl, 5 KCl, 0.4 $MgCl_2$, 1.8 $CaCl_2$, 1 D-glucose and 20 HEPES, and was adjusted to pH 7.4 and osmolarity of the medium cells were growing in. MES buffered saline solution (MBS) was prepared similarly by replacing HEPES with MES and adjusting the pH to 5.5 using NaOH. All salts were from Sigma Aldrich. HBS and MBS were perfused locally around the recorded cell using a 2-way borosilicate glass pipette. Movies were acquired at 0.5 Hz for a total of 900 seconds. For the first 120 s cells were imaged unstimulated, then quinpirole was added at a final concentration of 10 µM for 600 s, then quinpirole was washed out for the remaining 180 s.

Detection of endocytic events and their analyses were conducted using custom made Matlab scripts previously described (Jullié *et al*, 2014; Rosendale *et al*, 2017; Sposini *et al*, 2020), apart from kymographs which were obtained using ImageJ. Endocytic events are automatically detected, defined as sudden punctate fluorescence increase appearing in pH 5.5 images, visible for more than 3 frames (i.e. 8 seconds) and appeared at the same location as a pre-existing fluorescence cluster detectable in pH 7.4 images. Event frequency was expressed per cell surface area measured on the cell mask. Fluorescence quantification of events was performed as in (Sposini *et al*, 2020). In short, each value is calculated as the mean intensity in a 2-pixel radius circle centered on the detection to which the local background intensity is subtracted (the local background is taken as the 20th to 80th percentile of fluorescence in an annulus of 5 to 2 pixel outer and inner radii centred on the detection). The number and fluorescence of SEP-D2R clusters at pH 7.4 and the recruitment of βarr2-mCherry were analyzed by segmentation and tracking (multidimensional image analysis (MIA) developed for Metamorph by JB Sibarita, Bordeaux, France) as described in (Rosendale *et al*, 2019). Briefly, each image was segmented with a B-spline wavelet decomposition of scale 4 pixels and with a fixed threshold of eight times local standard deviation. Objects that could be tracked for more than three frames (6 s) were retained for further analysis with scripts written in Matlab 2018. The fluorescence value at each time point represents the average intensity in a 2 pixel (300 nm) radius circle around the centre of mass of the object to which the local

background intensity is subtracted. This local background is estimated in an annulus (5 pixel outer radius, 2 pixel inner radius) centred on the region to be quantified as the average intensity of pixel values between the 20th and 80th percentiles (to exclude neighbouring fluorescent objects). The frame of maximum intensity is used as the reference (time 0) for aligning and averaging all traces. Before (resp. after) tracking of an object the fluorescence is measured at the location of the first (resp. last) frame with the object tracked. Two colour alignment was performed using an image of beads (TetraSpeck microspheres, ThermoFisher) taken before the experiment.

Statistical analysis

Data are presented as mean ± SEM (standard error of the mean). Statistical significance was determined using GraphPad Prism 8.3.0 (GraphPad, La Jolla, CA, USA). Normality tests were performed with D'Agostino-Pearson omnibus tests. For non-normally distributed data, Kruskal-Wallis tests were used. Normally distributed data sets were analyzed using one-way ANOVA followed by Dunnett post-test more than two groups. Differences were considered significant at $p < 0.05$.

Acknowledgements

The authors are grateful to Prof. Jonathan Javitch for providing the FLAG-D2R construct and Dr Stefano Marullo for the β-arrestin2-mCherry construct. Imaging experiments were carried out at the Bordeaux Imaging Center, a service unit of the CNRS-INSERM and Bordeaux University, member of the national infrastructure France BioImaging supported by the French National Research Agency (ANR-10-INBS-04). We thank Magali Mondin for help with confocal microscopy. The work was supported by the ANR (LocalEndoProbes ANR-14-CE16-0012 and DopamineHub ANR-19-CE16-0003-01 to DP; polyFADO ANR-21-CE44-0019 to TD, PT, DP and IA; FrontoFat ANR-20-CE14-0020 to PT), University of Bordeaux's IdEx "Investments for the future" program/GPR BRAIN_2030 to DP and PT. SS is supported by a Sir Henry Wellcome postdoctoral fellowship (218650/Z/19/Z). RB PhD fellowship was obtained from the French "Ministère de l'Enseignement Supérieur et de la Recherche.

Author contributions

RB, SS, TD, PT, DP, IA designed the study. RB, SS, VDP, JH performed the experiments and analyses. TD, PT, DP, IA provided funding. RB, SS, PT, DP, IA wrote the initial versions of the manuscript. All authors edited the manuscript.

Conflict of interest

The authors declare no competing financial interests.

References

Baccouch R, Shi Y, Vernay E, Mathelié-Guinlet M, Taib-Maamar N, Villette S, Feuillie C, Rascol E, Nuss P, Lecomte S, *et al* (2023) The impact of lipid polyunsaturation on the physical and mechanical properties of lipid membranes. *Biochimica et Biophysica Acta (BBA) - Biomembranes* 1865: 184084

Barelli H & Antonny B (2016) Lipid unsaturation and organelle dynamics. *Current Opinion in Cell Biology* 41: 25–32

Bazinet RP & Layé S (2014) Polyunsaturated fatty acids and their metabolites in brain function and disease. *Nat Rev Neurosci* 15: 771–785

Beaulieu J-M & Gainetdinov RR (2011) The physiology, signaling, and pharmacology of dopamine receptors. *Pharmacol Rev* 63: 182–217

Beaulieu J-M, Sotnikova TD, Marion S, Lefkowitz RJ, Gainetdinov RR & Caron MG (2005) An Akt/beta-arrestin 2/PP2A signaling complex mediates dopaminergic neurotransmission and behavior. *Cell* 122: 261–273

Berger GE, Smesny S & Amminger GP (2006) Bioactive lipids in schizophrenia. *Int Rev Psychiatry* 18: 85–98

Boularan C, Scott MGH, Bourougaa K, Bellal M, Esteve E, Thuret A, Benmerah A, Tramier M, Coppey-Moisan M, Labbé-Jullié C, *et al* (2007) beta-arrestin 2 oligomerization controls the Mdm2-dependent inhibition of p53. *Proc Natl Acad Sci U S A* 104: 18061–18066

Calmet P, Cullin C, Cortès S, Vang M, Caudy N, Baccouch R, Dessolin J, Maamar NT, Lecomte S, Tillier B, *et al* (2020) Cholesterol impacts chemokine CCR5 receptor ligand-binding activity. *FEBS J* 287: 2367–2385

Chalon S (2006) Omega-3 fatty acids and monoamine neurotransmission. *Prostaglandins Leukot Essent Fatty Acids* 75: 259–269

Clayton CC, Donthamsetti P, Lambert NA, Javitch JA & Neve KA (2014) Mutation of three residues in the third intracellular loop of the dopamine D2 receptor creates an internalization-defective receptor. *J Biol Chem* 289: 33663–33675

Dawaliby R, Trubbia C, Delporte C, Masureel M, Van Antwerpen P, Kobilka BK & Govaerts C (2016) Allosteric regulation of G protein-coupled receptor activity by phospholipids. *Nat Chem Biol* 12: 35–39

Del'guidice T, Lemasson M & Beaulieu J-M (2011) Role of Beta-arrestin 2 downstream of dopamine receptors in the Basal Ganglia. *Front Neuroanat* 5: 58

Doherty GJ & McMahon HT (2009) Mechanisms of Endocytosis. *Annual Review of Biochemistry* 78: 857–902

Ducrocq F, Walle R, Contini A, Oummadi A, Carabaño B, van der Veldt S, Boyer M-L, Aby F, Tolentino-Cortez T, Helbling J-C, *et al* (2020) Causal Link between n-3 Polyunsaturated Fatty Acid Deficiency and Motivation Deficits. *Cell Metabolism* 31: 755-772.e7

Eichel K, Jullié D, Barsi-Rhyne B, Latorraca NR, Masureel M, Sibarita J-B, Dror RO & von Zastrow M (2018) Catalytic activation of β-arrestin by GPCRs. *Nature* 557: 381–386

Fallahi-Sichani M & Linderman JJ (2009) Lipid raft-mediated regulation of G-protein coupled receptor signaling by ligands which influence receptor dimerization: a computational study. *PLoS One* 4: e6604

Folch J, Lees M & Sloane Stanley GH (1957) A simple method for the isolation and purification of total lipides from animal tissues. *J Biol Chem* 226: 497–509

Garland MR, Hallahan B, McNamara M, Carney PA, Grimes H, Hibbeln JR, Harkin A & Conroy RM (2007) Lipids and essential fatty acids in patients presenting with self-harm. *Br J Psychiatry* 190: 112–117

Goodman OB, Krupnick JG, Santini F, Gurevich VV, Penn RB, Gagnon AW, Keen JH & Benovic JL (1996) Beta-arrestin acts as a clathrin adaptor in endocytosis of the beta2-adrenergic receptor. *Nature* 383: 447–450

Grimes J, Koszegi Z, Lanoiselée Y, Miljus T, O'Brien SL, Stepniewski TM, Medel-Lacruz B, Baidya M, Makarova M, Mistry R, *et al* (2023) Plasma membrane preassociation drives β-arrestin coupling to receptors and activation. *Cell* 186: 2238-2255.e20

Grossfield A, Feller SE & Pitman MC (2006) A role for direct interactions in the modulation of rhodopsin by omega-3 polyunsaturated lipids. *Proc Natl Acad Sci U S A* 103: 4888–4893

Grosso G, Pajak A, Marventano S, Castellano S, Galvano F, Bucolo C, Drago F & Caraci F (2014) Role of omega-3 fatty acids in the treatment of depressive disorders: a comprehensive meta-analysis of randomized clinical trials. *PLoS One* 9: e96905

Guixà-González R, Javanainen M, Gómez-Soler M, Cordobilla B, Domingo JC, Sanz F, Pastor M, Ciruela F, Martinez-Seara H & Selent J (2016) Membrane omega-3 fatty acids modulate the oligomerisation kinetics of adenosine A2A and dopamine D2 receptors. *Sci Rep* 6: 19839

Guo W, Urizar E, Kralikova M, Mobarec JC, Shi L, Filizola M & Javitch JA (2008) Dopamine D2 receptors form higher order oligomers at physiological expression levels. *EMBO J* 27: 2293–2304

Gurevich VV & Gurevich EV (2006) The structural basis of arrestin-mediated regulation of G-protein-coupled receptors. *Pharmacol Ther* 110: 465–502

Janetzko J, Kise R, Barsi-Rhyne B, Siepe DH, Heydenreich FM, Kawakami K, Masureel M, Maeda S, Garcia KC, von Zastrow M, *et al* (2022) Membrane phosphoinositides regulate GPCR-β-arrestin complex assembly and dynamics. *Cell* 185: 4560-4573.e19

Jastrzebska B, Debinski A, Filipek S & Palczewski K (2011) Role of membrane integrity on G protein-coupled receptors: Rhodopsin stability and function. *Prog Lipid Res* 50: 267–277

Jean-Alphonse FG & Sposini S (2021) Confocal and TIRF microscopy based approaches to visualize arrestin trafficking in living cells. *Methods Cell Biol* 166: 179–203

Jobin M-L, De Smedt-Peyrusse V, Ducrocq F, Baccouch R, Oummadi A, Pedersen MH, Medel-Lacruz B, Angelo M-F, Villette S, Van Delft P, *et al* (2023) Impact of membrane lipid polyunsaturation on dopamine D2 receptor ligand binding and signaling. *Mol Psychiatry* 28: 1960–1969

Joffre C, Grégoire S, De Smedt V, Acar N, Bretillon L, Nadjar A & Layé S (2016) Modulation of brain PUFA content in different experimental models of mice. *Prostaglandins, Leukotrienes and Essential Fatty Acids* 114: 1–10

Jullié D, Choquet D & Perrais D (2014) Recycling Endosomes Undergo Rapid Closure of a Fusion Pore on Exocytosis in Neuronal Dendrites. *Journal of Neuroscience* 34: 11106–11118

Kim KM, Valenzano KJ, Robinson SR, Yao WD, Barak LS & Caron MG (2001) Differential regulation of the dopamine D2 and D3 receptors by G protein-coupled receptor kinases and beta-arrestins. *J Biol Chem* 276: 37409–37414

Komolov KE, Du Y, Duc NM, Betz RM, Rodrigues JPGLM, Leib RD, Patra D, Skiniotis G, Adams CM, Dror RO, *et al* (2017) Structural and Functional Analysis of a β2-Adrenergic Receptor Complex with GRK5. *Cell* 169: 407-421.e16

Lan H, Liu Y, Bell MI, Gurevich VV & Neve KA (2009) A dopamine D2 receptor mutant capable of G protein-mediated signaling but deficient in arrestin binding. *Mol Pharmacol* 75: 113–123

Leonard AN & Lyman E (2021) Activation of G-protein-coupled receptors is thermodynamically linked to lipid solvation. *Biophys J* 120: 1777–1787

Levoye A, Zwier JM, Jaracz-Ros A, Klipfel L, Cottet M, Maurel D, Bdioui S, Balabanian K, Prézeau L, Trinquet E, *et al* (2015) A broad G protein-coupled receptor internalization assay that combines SNAP-tag labeling, diffusion-enhanced resonance energy transfer, and a highly emissive terbium cryptate. *Frontiers in Endocrinology* 6

Manni MM, Tiberti ML, Pagnotta S, Barelli H, Gautier R & Antonny B (2018) Acyl chain asymmetry and polyunsaturation of brain phospholipids facilitate membrane vesiculation without leakage. *eLife* 7: e34394

McNamara RK, Hahn C-G, Jandacek R, Rider T, Tso P, Stanford KE & Richtand NM (2007a) Selective deficits in the omega-3 fatty acid docosahexaenoic acid in the postmortem orbitofrontal cortex of patients with major depressive disorder. *Biol Psychiatry* 62: 17–24

McNamara RK, Jandacek R, Rider T, Tso P, Hahn C-G, Richtand NM & Stanford KE (2007b) Abnormalities in the fatty acid composition of the postmortem orbitofrontal cortex of schizophrenic patients: gender differences and partial normalization with antipsychotic medications. *Schizophr Res* 91: 37–50

McNamara RK, Jandacek R, Rider T, Tso P, Stanford KE, Hahn C-G & Richtand NM (2008) Deficits in docosahexaenoic acid and associated elevations in the metabolism of arachidonic acid and saturated fatty acids in the postmortem orbitofrontal cortex of patients with bipolar disorder. *Psychiatry Res* 160: 285–299

Mitchell DC, Straume M & Litman BJ (1992) Role of sn-1-saturated,sn-2-polyunsaturated phospholipids in control of membrane receptor conformational equilibrium: effects of cholesterol and acyl chain unsaturation on the metarhodopsin I in equilibrium with metarhodopsin II equilibrium. *Biochemistry* 31: 662–670

Mizumura T, Kondo K, Kurita M, Kofuku Y, Natsume M, Imai S, Shiraishi Y, Ueda T & Shimada I (2020) Activation of adenosine A2A receptor by lipids from docosahexaenoic acid revealed by NMR. *Sci Adv* 6: eaay8544

Monastyrskaya K, Hostettler A, Buergi S & Draeger A (2005) The NK1 receptor localizes to the plasma membrane microdomains, and its activation is dependent on lipid raft integrity. *J Biol Chem* 280: 7135–7146

Morrison WR & Smith LM (1964) PREPARATION OF FATTY ACID METHYL ESTERS AND DIMETHYLACETALS FROM LIPIDS WITH BORON FLUORIDE--METHANOL. *J Lipid Res* 5: 600–608

Niu S-L, Mitchell DC, Lim S-Y, Wen Z-M, Kim H-Y, Salem N & Litman BJ (2004) Reduced G protein-coupled signaling efficiency in retinal rod outer segments in response to n-3 fatty acid deficiency. *J Biol Chem* 279: 31098–31104

Oh P & Schnitzer JE (2001) Segregation of heterotrimeric G proteins in cell surface microdomains. G(q) binds caveolin to concentrate in caveolae, whereas G(i) and G(s) target lipid rafts by default. *Mol Biol Cell* 12: 685–698

Paspalas CD, Rakic P & Goldman-Rakic PS (2006) Internalization of D2 dopamine receptors is clathrin-dependent and select to dendro-axonic appositions in primate prefrontal cortex. *Eur J Neurosci* 24: 1395–1403

Pinot M, Vanni S, Pagnotta S, Lacas-Gervais S, Payet L-A, Ferreira T, Gautier R, Goud B, Antonny B & Barelli H (2014) Polyunsaturated phospholipids facilitate membrane deformation and fission by endocytic proteins. *Science* 345: 693–697

Pluhackova K, Wilhelm FM & Müller DJ (2021) Lipids and Phosphorylation Conjointly Modulate Complex Formation of β2-Adrenergic Receptor and β-arrestin2. *Front Cell Dev Biol* 9: 807913

Pontier SM, Percherancier Y, Galandrin S, Breit A, Galés C & Bouvier M (2008) Cholesterol-dependent separation of the beta2-adrenergic receptor from its partners determines signaling efficacy: insight into nanoscale organization of signal transduction. *J Biol Chem* 283: 24659–24672

Pucadyil TJ & Chattopadhyay A (2004) Cholesterol modulates ligand binding and G-protein coupling to serotonin 1A receptors from bovine hippocampus. 1663: 188–200

Robinson BG, Bunzow JR, Grimm JB, Lavis LD, Dudman JT, Brown J, Neve KA & Williams JT (2017) Desensitized D2 autoreceptors are resistant to trafficking. *Scientific Reports* 7: 4379

Robinson DG, Gallego JA, John M, Hanna LA, Zhang J-P, Birnbaum ML, Greenberg J, Naraine M, Peters BD, McNamara RK, *et al* (2019) A potential role for adjunctive omega-3 polyunsaturated fatty acids for depression and anxiety symptoms in recent onset psychosis: Results from a 16 week randomized placebo-controlled trial for participants concurrently treated with risperidone. *Schizophr Res* 204: 295–303

Rosendale M, Jullié D, Choquet D & Perrais D (2017) Spatial and Temporal Regulation of Receptor Endocytosis in Neuronal Dendrites Revealed by Imaging of Single Vesicle Formation. *Cell Reports* 18: 1840–1847

Rosendale M, Van TNN, Grillo-Bosch D, Sposini S, Claverie L, Gauthereau I, Claverol S, Choquet D, Sainlos M & Perrais D (2019) Functional recruitment of dynamin requires multimeric interactions for efficient endocytosis. *Nat Commun* 10: 4462

Skinbjerg M, Ariano MA, Thorsell A, Heilig M, Halldin C, Innis RB & Sibley DR (2009) Arrestin3 mediates D(2) dopamine receptor internalization. *Synapse* 63: 621–624

Sommer ME, Smith WC & Farrens DL (2006) Dynamics of arrestin-rhodopsin interactions: acidic phospholipids enable binding of arrestin to purified rhodopsin in detergent. *J Biol Chem* 281: 9407–9417

Soubias O, Teague WE & Gawrisch K (2006) Evidence for specificity in lipid-rhodopsin interactions. *J Biol Chem* 281: 33233–33241

Sposini S & Hanyaloglu AC (2018) Evolving View of Membrane Trafficking and Signaling Systems for G Protein-Coupled Receptors. *Prog Mol Subcell Biol* 57: 273–299

Sposini S, Jean-Alphonse FG, Ayoub MA, Oqua A, West C, Lavery S, Brosens JJ, Reiter E & Hanyaloglu AC (2017) Integration of GPCR Signaling and Sorting from Very Early Endosomes via Opposing APPL1 Mechanisms. *Cell Reports* 21: 2855–2867

Sposini S, Rosendale M, Claverie L, Van TNN, Jullié D & Perrais D (2020) Imaging endocytic vesicle formation at high spatial and temporal resolutions with the pulsed-pH protocol. *Nature Protocols* 15, pages: 3088–3104

Taylor MJ, Perrais D & Merrifield CJ (2011) A High Precision Survey of the Molecular Dynamics of Mammalian Clathrin-Mediated Endocytosis. *PLoS Biology* 9: e1000604

Thakur N, Ray AP, Sharp L, Jin B, Duong A, Pour NG, Obeng S, Wijesekara AV, Gao Z-G, McCurdy CR, *et al* (2023) Anionic phospholipids control mechanisms of GPCR-G protein recognition. *Nat Commun* 14: 794

Tsao P & von Zastrow M (2000) Downregulation of G protein-coupled receptors. *Curr Opin Neurobiol* 10: 365–369

Villar VAM, Cuevas S, Zheng X & Jose PA (2016) Localization and signaling of GPCRs in lipid rafts. *Methods Cell Biol* 132: 3–23

Whitton AE, Treadway MT & Pizzagalli DA (2015) Reward processing dysfunction in major depression, bipolar disorder and schizophrenia. *Curr Opin Psychiatry* 28: 7–12

Xu P, Huang S, Zhang H, Mao C, Zhou XE, Cheng X, Simon IA, Shen D-D, Yen H-Y, Robinson CV, *et al* (2021) Structural insights into the lipid and ligand regulation of serotonin receptors. *Nature* 592: 469–473

Yang L & Lyman E (2019) Local Enrichment of Unsaturated Chains around the A2A Adenosine Receptor. *Biochemistry* 58: 4096–4105

von Zastrow M & Kobilka BK (1994) Antagonist-dependent and -independent steps in the mechanism of adrenergic receptor internalization. *J Biol Chem* 269: 18448–18452

Figures

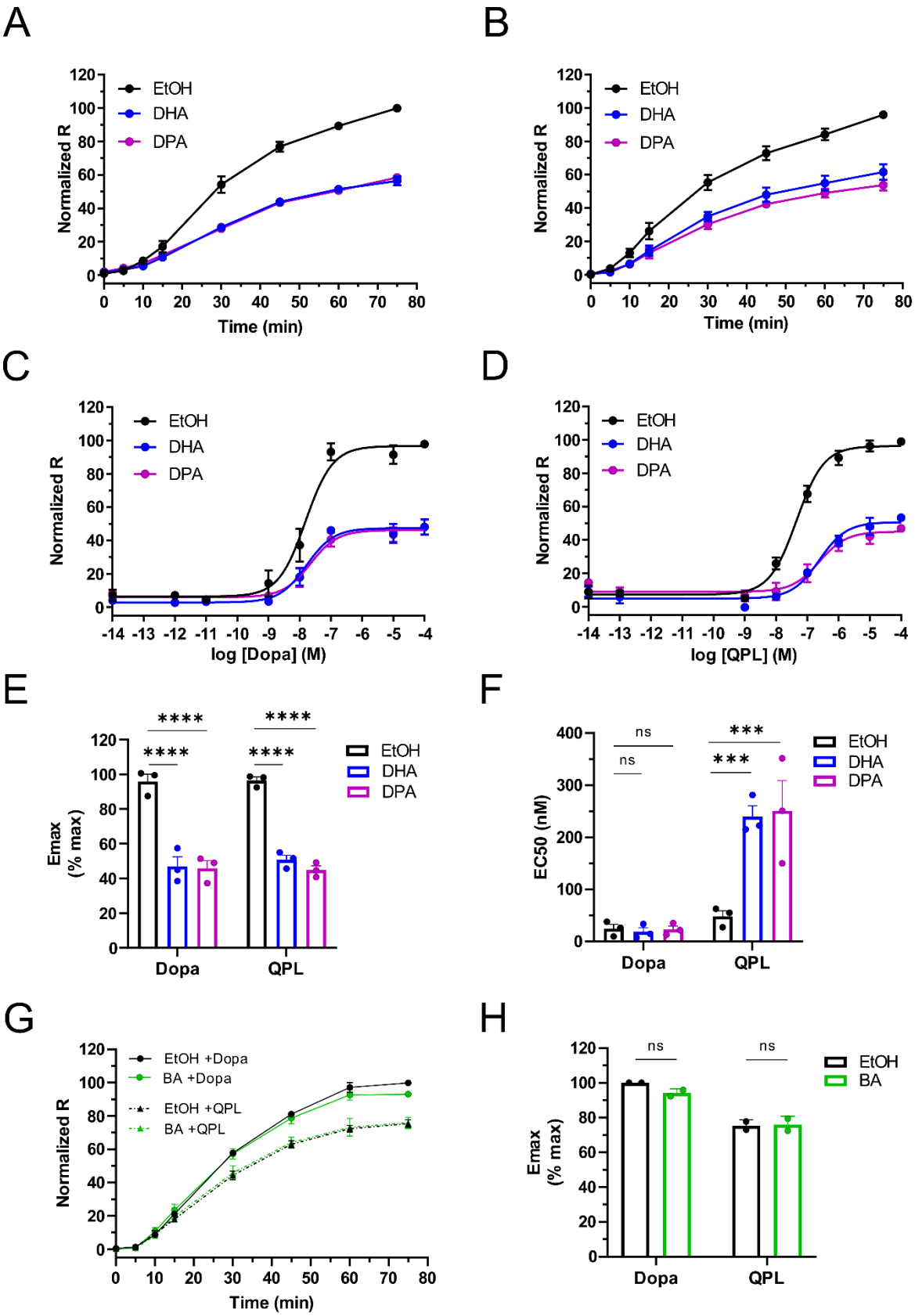

Figure 1: Impact of PUFAs on D2R induced internalization investigated by DERET assay. A, **B**: Real-time internalization of SNAP tagged D2R upon Dopamine (A) or

Quinpirole (B) stimulation (10 µM) of non-enriched (control) and PUFAs (ω3, DHA and ω6, DPA) enriched cells. Percentage of fluorescence ratio (ratio of the donor/acceptor fluorescence intensity; 620/520 nm) were plotted as a function of time. **C, D:** Dose–response curves of D2R agonist (Dopa, C; QPL, D) induced internalization following 30 min incubation at 37°C in presence of an increasing concentrations of the indicated agonist. Data were fitted using non-linear regression dose–response and expressed as log [ligand] *versus* response for the 3 different conditions. **E, F:** Emax and EC_{50} values obtained from dose-response experiments of D2R internalization (C and D). **G:** Real-time internalization of SNAP tagged D2R expressed in ethanol (EtOH) and behenic acid (BA)-enriched cells upon stimulation with 10 µM of dopamine or quinpirole. **H**: Emax values measured in control and BA-enriched cells 30 min after dopamine or quinpirole stimulation. n= 3 independent experiments carried out in triplicates. Two-way ANOVA test with Sidak's multiple comparisons test; **** $p < 0.0001$, *** $p < 0.001$, ns $p \geq 0.05$.

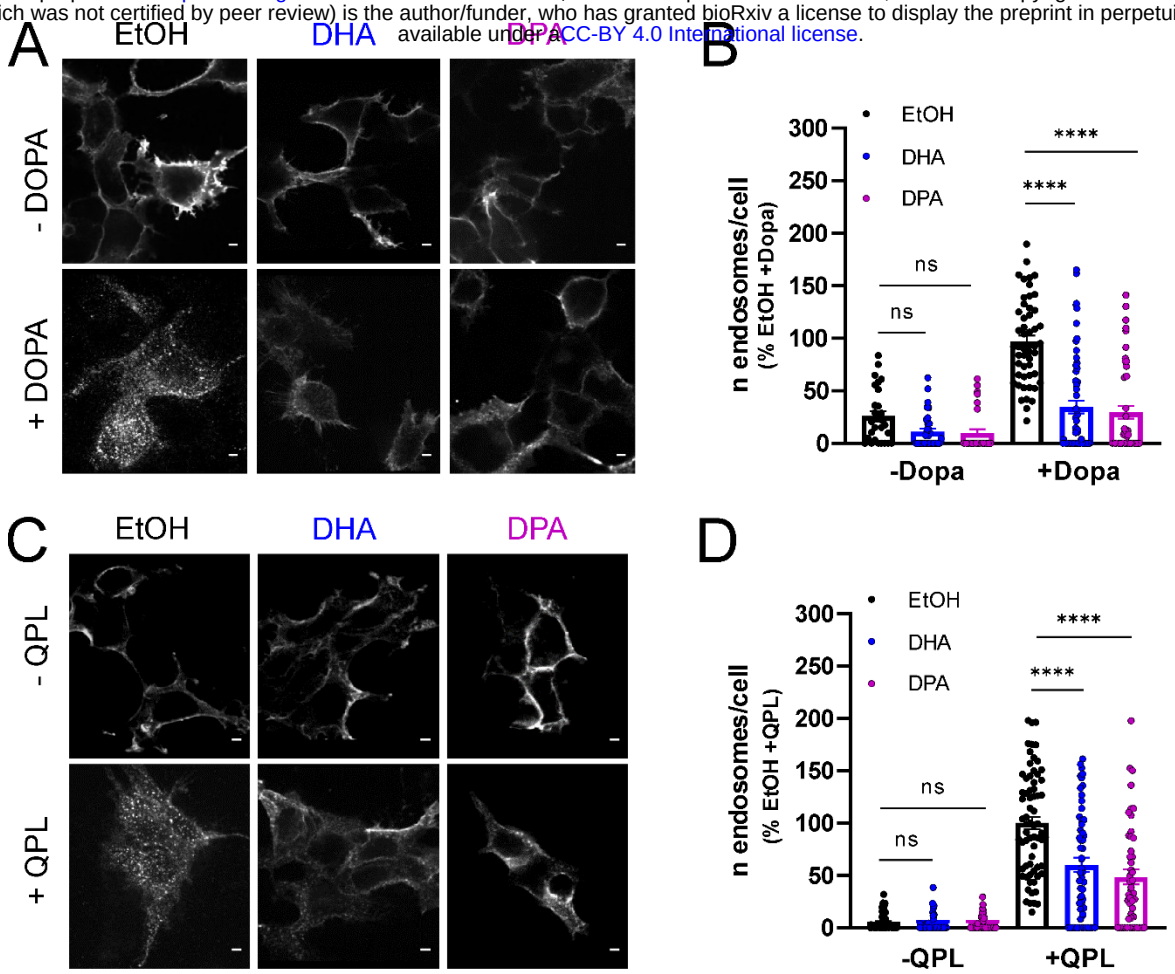

Figure 2: PUFA enrichment affects D2R internalization. **A, C:** Representative confocal microscopy images of Flag-D2R expressing HEK293 cells enriched in either ethanol (EtOH), DHA or DPA, before and after stimulation with either 10 µM of Dopamine (Dopa) (A) or 10 µM of Quinpirole (QPL) (C) for 30 min. Scale bar = 5 µm. **B, D**: Quantification of D2R endosomes generated before and after dopamine (Dopa) (B) or quinpirole (QPL) (D) stimulation in control and PUFAs enriched cells. n= 68-71 per condition collected across 3 independent experiments. One-way ANOVA with Dunnett's multiple comparisons test; ****p<0.0001, ***p<0.001, ns p≥0.05.

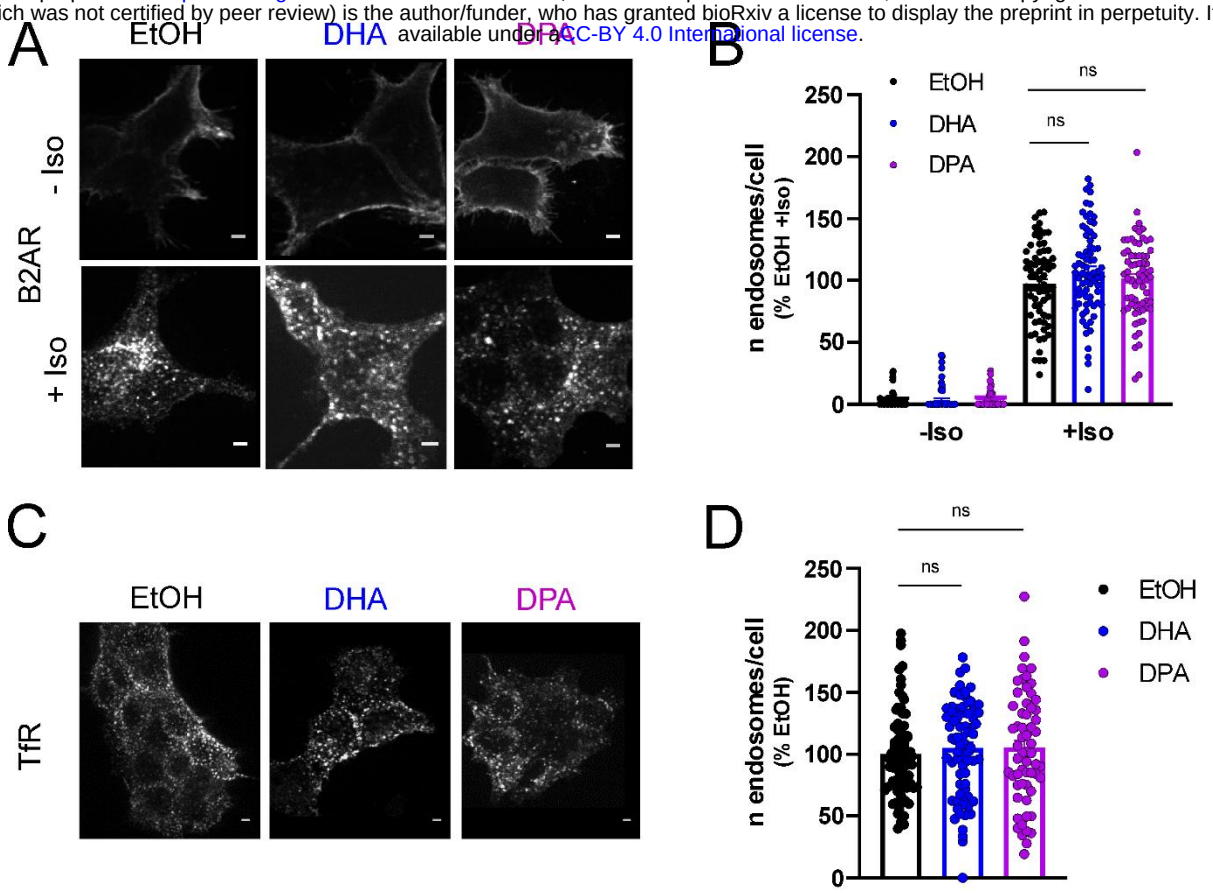

Figure 3: PUFAs do not alter internalization of the class A GPCR β2AR nor Transferrin uptake. **A:** Representative confocal microscopy images of Flag-β2AR expressing HEK293 cells enriched in either ethanol (EtOH), DHA or DPA, before and after stimulation with 10 µM of Isoproterenol (ISO) for 30 min. Scale bar = 5 µm. **B:** Quantification of β2AR endosomes in stimulated cells from (A); n = 64-74 cells per condition collected across 3 independent experiments. One-way ANOVA with Dunnett's multiple comparisons test: ns $p \geq 0.05$. **C**: Representative confocal microscopy images of HEK293 cells enriched in either ethanol (EtOH), DHA or DPA, incubated with fluorescently labeled transferrin for 5 min at 37 °C. Scale bar = 5 µm. **D:** Quantification of TfR endosomes; n= 64-74 cells per condition from 3 independent experiments. One-one-way ANOVA with Dunnett's multiple comparisons test: ns $p \geq 0.05$.

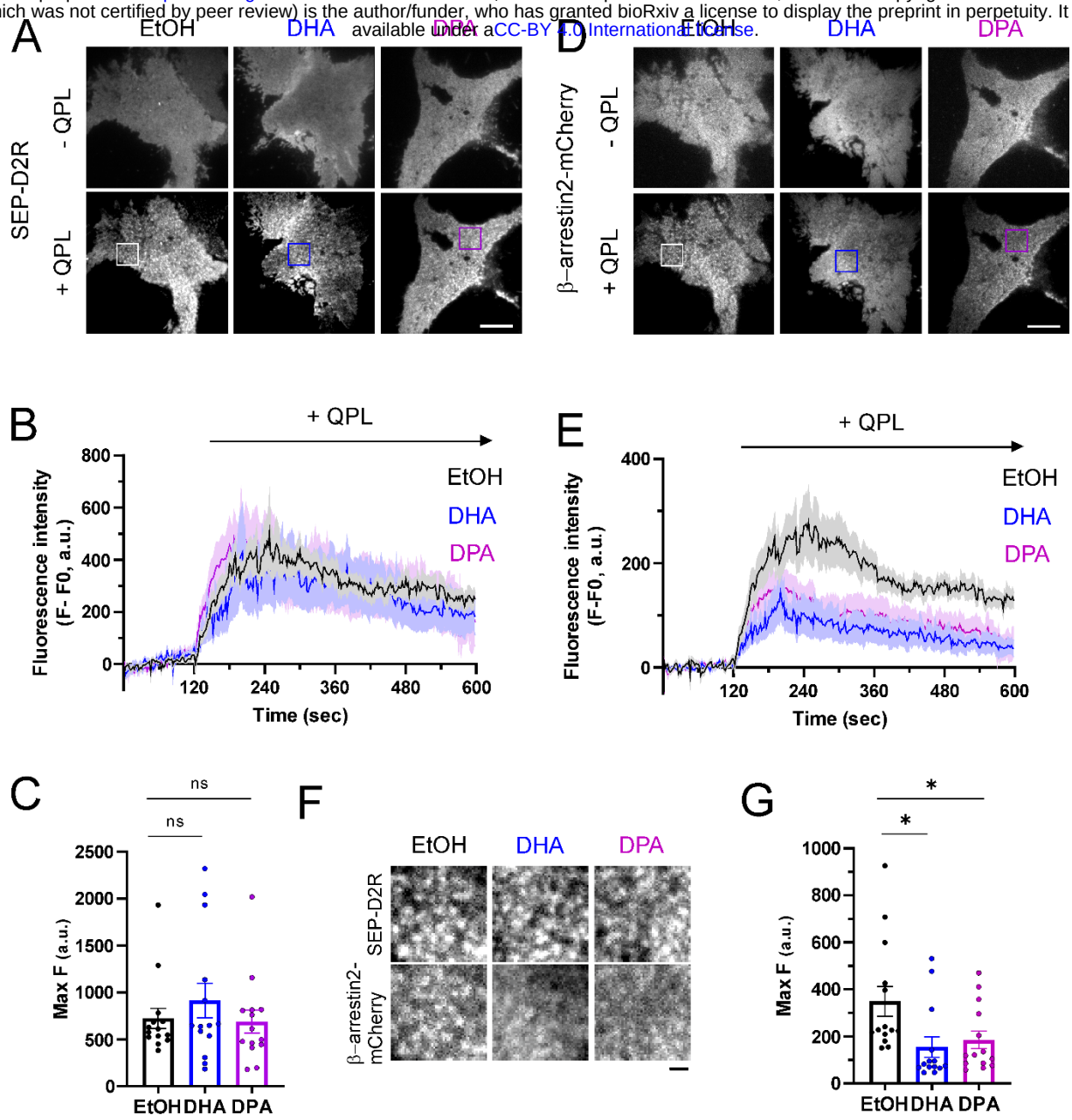

Figure 4: PUFA enrichment does not affect D2R clustering but impairs the recruitment of β-arrestin2 upon Quinpirole addition. A, D: Representative TIRF microscopy images of HEK293 cells co-expressing SEP-D2R, GRK2 and β-arrestin2-mCherry enriched in either ethanol (EtOH), DHA or DPA, showing the pattern of expression at the plasma membrane for SEP-D2R (A) and β-arrestin2-mCherry (D) before and after stimulation with 10 µM of Quinpirole (QPL). Scale bar= 5 µm. See also Movies EV1-3. **B, E:** Mean Fluorescence intensity profiles of SEP-D2R (B) and β-arrestin 2-mCherry (E) obtained before and after quinpirole (QPL) addition at t=120 s. Data represent average fluorescence values within an ROI drawn around each cluster minus background fluorescence (= fluorescence measured in the ROI during the 60 frames before agonist addition was averaged and subtracted from fluorescence values at each frame). **C, G:** Maximum fluorescence intensities of SEP-D2R (C) and β-arrestin2-mCherry (F) measured after quinpirole addition. Values represent maximum intensity fluorescence minus background fluorescence in each ROI for n= 14 cells per condition collected across 3 independent experiments. One-way ANOVA test with Dunnett's

multiple comparisons test; * $p < 0.05$, ns $p \geq 0.05$. **F.** Zoom-in images taken from panels in A and D, as shown by ROIs, depicting SEP-D2R and β-arrestin2-mCherry clusters after quinpirole addition. Scale bar= 1 µm.

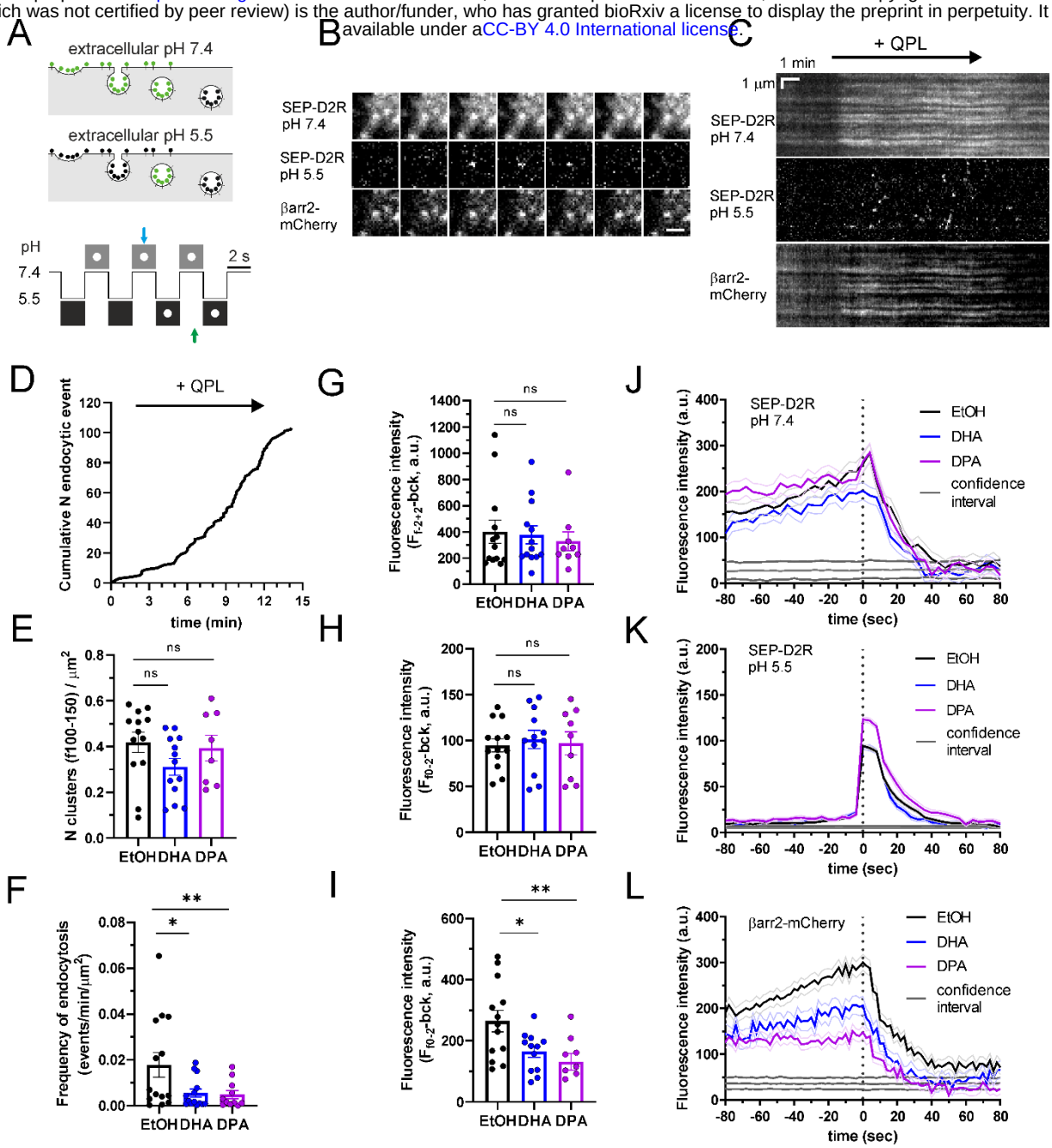

Figure 5: Reduction of endocytic vesicle formation and recruitment of β-arrestin2 at nascent D2R endocytic vesicles in PUFA enriched cells. A: Top, experimental procedure: a cell expressing SEP-D2R is bathed in solutions alternating between pH 7.4 and 5.5. At pH 7.4, SEP-D2R on the plasma membrane and in non-acidic vesicles is visible (green lollipops). At pH 5.5, the surface receptors are not fluorescent (black lollipops), and the fluorescence from non-acidic CCVs is isolated. Bottom, principle of vesicle detection: a CCV formed at pH 7.4 (blue arrow) will be visible on the next image at pH 5.5 (green arrow). **B:** Example of a D2R cluster (top row), the corresponding endocytic event (middle row) and the associated β-arrestin2 cluster (bottom row) detected with the ppH protocol. Scale bar= 1 µm. **C:** Kymographs from a representative TIRF microscopy movie (EV Movie 4) of a HEK293 cells transfected with SEP-D2R, β-arrestin2-mCherry and GRK2 and imaged live with the ppH protocol before (t=0-120 s), during (t=121-720 s) and after (t=701-900 s) application of 10 µM Quinpirole (QPL). **D:** Cumulative number of endocytic events detected with the ppH

protocol in a representative HEK293 cell transfected and imaged as in C and shown in movie EV4. **E:** Number of D2R clusters/cell detected during Quinpirole application in cells transfected as in C, treated with either EtOH, DHA or DPA and imaged live with the ppH protocol. One-way ANOVA with Dunnett's multiple comparisons test of n= 13, 13 and 8 cells treated with EtOH, DHA or DPA, respectively; ns $p \geq 0.05$ **F:** Number of endocytic events/cell detected during Quinpirole application in cells transfected as in C, treated with either EtOH, DHA or DPA and imaged live with the ppH protocol. One-way ANOVA with Dunnett's multiple comparisons test of n= 14, 14 and 11 cells treated with EtOH, DHA or DPA, respectively; ** $p < 0.01$, * $p < 0.05$. **G-I:** Average fluorescence intensity of all events in a given cell, at the time of endocytic event detection, for SEP-D2R at pH7.4 (G), SEP-D2R at pH 5.5 (H) and β-arrestin2-mCherry at pH 5.5 (I) obtained from cells transfected and imaged as in C. One-way ANOVA test with Dunnett's multiple comparisons test for n= 13, 12 and 9 cells treated with EtOH, DHA and DPA, respectively; ** $p < 0.01$, * $p < 0.05$, ns $p \geq 0.05$. **J-L:** Average fluorescence over time of SEP-D2R at pH 7.4 (J), SEP-D2R at pH 5.5 (K) and β-arrestin2-mCherry at pH 5.5 (L), aligned to the time of vesicle scission (t = 0 s) obtained from terminal events (events for which the SEP-D2R cluster at pH 7.4 disappears within 80 s, defined as in (Taylor *et al*, 2011; Sposini *et al*, 2020) for the same cells used in G-I. Black lines represent 95% confidence intervals for randomized events to determine the level of enrichment at sites of scission. N = 424 terminal events from 13 cells (EtOH), 191 terminal events from 12 cells (DHA) and 254 terminal events from 9 cells (DPA).

Reagents and Tools Table

Reagent or tool	Source	Identifier
Antibodies		
Anti-FLAG M1 antibody	Sigma	F3040
Alexa Fluor 555 anti-mouse antibody	ThermoFisher Scientific	A31570
Alexa Fluor 568-Tfn	ThermoFisher Scientific	T23365
Buffers		
PBS		
DMEM	ThermoFisher Scientific	10564-011
FluoroBrite DMEM	ThermoFisher Scientific	A1896701
Tag-lite buffer	Revvity	LABMED
Chemicals, peptides and recombinant proteins		
Dopamine	Sigma	H8502
Quinpirole	Sigma	Q102
Haloperidol	Sigma	H1512
Aripiprazole	Sigma	SML0935
Docosahexaenoic acid, DHA	Sigma	D2534
Docosapentaenoic acid, DPA	Sigma	18566
Behenic acid, BA	Sigma	216941
Isoproterenol	Sigma	I6504
TetraSpeck microspheres	ThermoFisher	T7280
Fluoromount-G	ThermoFisher	00-4958-02
Experimental models: cell lines		
HEK-293 cells	ECACC	12022001
Oligonucleotides		
FW (5'-3')	tgttcgccgactacaagaccggtgatgacgccatggatcc	
REV (5'-3')	ggatccatggcgtcatcaccggtcttgtagtcggcgaaca	
Recombinant DNA		
SEP-D2R	This study	
FLAG-D2R	Prof. Jonathan Javitch, Columbia University	
FLAG-B2AR	Prof. Aylin Hanyaloglu, Imperial College London	
βarrestin2-mCherry	Dr. Stefano Marullo, Institut Cochin	(Boularan *et al*, 2007)
Software and algorithms		
Metamorph 7.10	https://www.moleculardevices.com/products/cellular-imaging-systems/acquisition-and-analysis-software/metamorph-microscopy	N/A
MATLAB 2018b	https://fr.mathworks.com	N/A
Custom MATLAB scripts	Scission_analysis (Sposini *et al*, 2020)	MATLAB Central File Exchange 72744-

		scission_analysis
ImageJ 1.53c	http://www.imagej.nih.gov/ij	N/A
Galaxie	Varian	
Kits		
QuickChange Mutagenesis kit	Agilent	200519

A

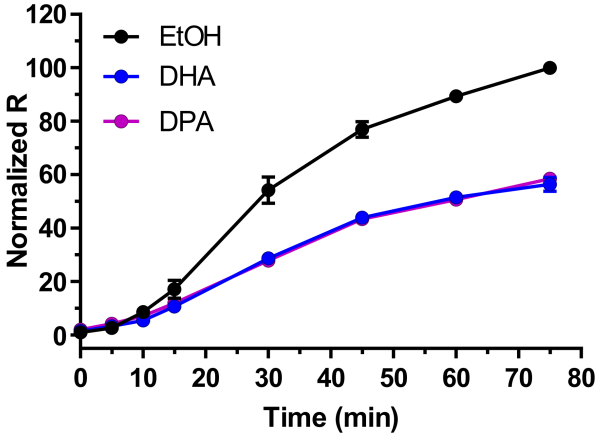

B

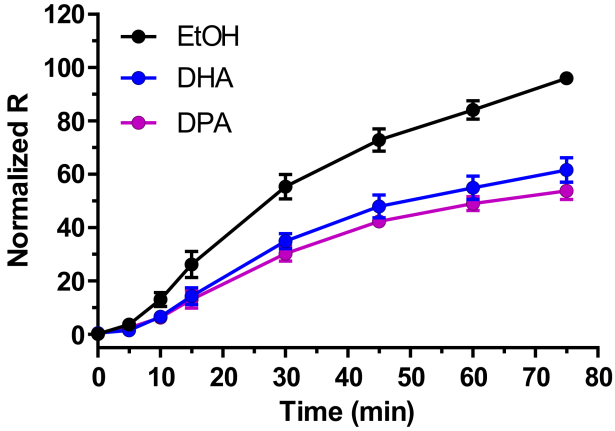

C

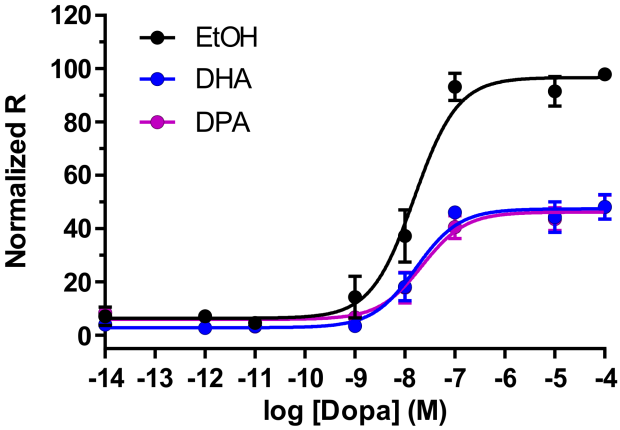

D

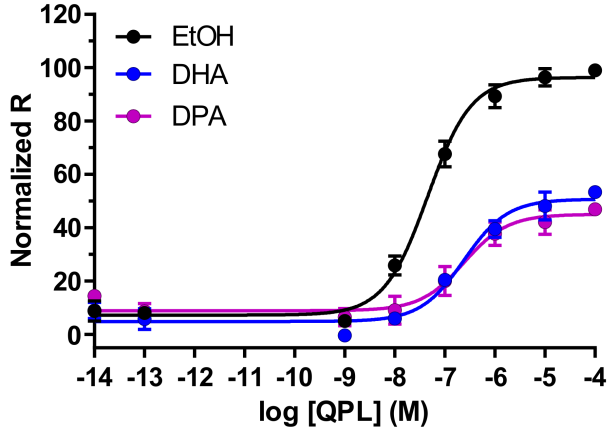

E

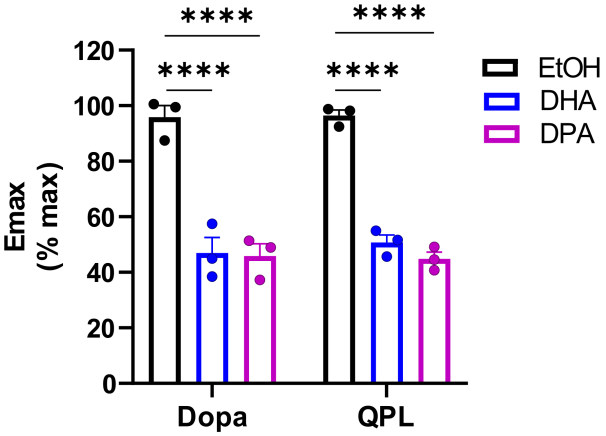

F

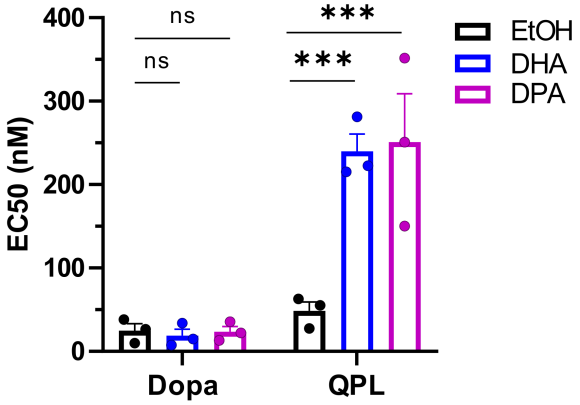

G

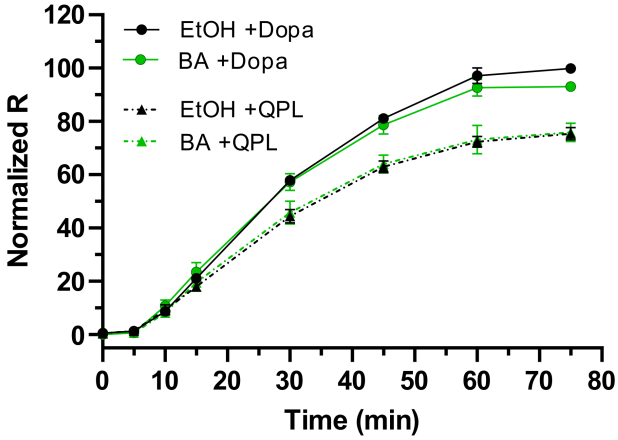

H